Proceedings of the ASME Turbo Expo 2015: Turbine Technical Conference and Exposition
GT2015
June 15-19, 2015, Montreal, Canada

GT2015-43219

DRAFT: HEAT RELEASE RESPONSE TO FORCED FLOW OSCILLATIONS OF A LOW-ORDER MODELLED LABORATORY SCALE DUMP COMBUSTOR

Alessandro Orchini* **Matthew P. Juniper**
Department of Engineering
University of Cambridge
Trumpington Street, CB2 1PZ, Cambridge, UK

ABSTRACT

In this study we investigate the heat release response to forced harmonic velocity fluctuations of a bluff body dump combustor. We use the kinematic G-equation as a low-order model for the flame and heat release dynamics. The geometry considered is based on an experimental setup developed by R. Balachandran and widely investigated in the literature, and we look for a qualitative comparison with experimental and numerical results. We model the flow field dynamics adapting the well-known travelling wave model, which was originally developed for conical flames, to the case of a bluff-body stabilized flame in a non-uniform mean flow field. We impose velocity fluctuations at the dump plane at various frequencies and amplitudes and we integrate the nonlinear flame and heat release dynamics. Results show that the model qualitatively reproduces the kinematic behaviour observed in the experiments, although some major quantitative differences are found. We conclude by discussing our results, and adjustments that could be introduced in future in the low-order model in order to improve it.

NOMENCLATURE

G Scalar field
$G = 0$ Flame front
$\boldsymbol{u}$ Flow field
s_L Flame speed
s_L^0 Unstretched flame speed
$\mathscr{L}$ Markstein length
$\hat{\boldsymbol{n}}$ Flame normal
κ Flame curvature
ϕ Equivalence ratio
$\bar{\cdot}$ Mean quantities
$\cdot'$ Fluctuating quantities
f Forcing frequency
A Forcing amplitude
Q Total heat release
$\mathscr{F}$ Flame Describing Function

INTRODUCTION

Low-order modelling is very important in thermoacoustics. Although it relies on radical (but physically-based) approximations in the flame-flow-acoustic coupling, it allows for a huge reduction of the degrees of freedom needed to describe the thermoacoustic interaction. As the computational cost required to integrate the system is highly reduced, low-order models can be used to investigate a large variety of parameters and gain insight into the physical mechanisms that cause thermoacoustic oscillations to arise.

For premixed flames, the kinematic G-equation is a common model used to determine the position and evolution of a thin flame front, as well as the amount of heat released by the flame. In the linear limit, transfer functions of conical and V shaped flames to harmonic velocity and heat release fluctuations have been evaluated analytically for a variety of underlying flow fields [1, 2]. In particular, a travelling wave model for flow perturbations has been shown to accurately reproduce the flow-flame

*Email: ao352@cam.ac.uk. Address all correspondence to this author.

interaction. Also, transfer functions of heat release fluctuations to harmonic velocity disturbances for these flame shapes have been proven to match experimental results [3]. In the nonlinear regime, 2-dimensional tent and axisymmetric conical flames have been investigated with a variety of tools both in the frequency and time domain. Frequency domain analyses are based on the Flame Describing Function [4,5], and allow for the prediction of frequencies and amplitudes of oscillations when the oscillations are associated with a single thermoacoustic mode. Time domain analyses allow for a more extensive investigation of thermoacoustic systems, and phenomena linked to the nonlinear dynamical nature of the system, such as period-doubling, secondary Hopf bifurcations, and routes to chaos, can be observed [6, 7, 8].

In this study, we extend the models derived for conical flames to a more realistic combustor configuration. The combustor we investigate is a dump combustor which has been developed by Balachandran [9], and is shown in Figure 1. As the experiments performed on this setup represent one of the first set of measurements of forced turbulent flames in the nonlinear regime, low-order and CFD simulations of this rig have already been performed. In [10] a G-equation based low-order model has been developed. However, in that study the flow field was treated as a potential flow generated by a pulsating spherical source upstream of the bluff body. This does not include the characteristic formation of vortices at the slot and their roll up. Also, each side of the flame was treated explicitly as a single-valued function in one of the coordinates; this condition is not necessarily satisfied if the flame shape becomes very wrinkled. More accurate numerical simulations based on unsteady Reynolds-averaged Navier–Stokes (URANS) models were performed by [11, 12].

Our goal is to develop a low-order model based on the fully implicit G-equation that describes the flame-flow interaction in this configuration. The implicit formulation naturally includes the possibility for the flame to assume configurations that are not necessarily single-valued in any simple coordinate system. The flame is stabilized by a bluff body, and, although it resembles the structure of a V-flame, it differs from it in the fact that the reactants are enclosed between inner and outer flame surfaces, which are assumed to be axisymmetric. The flame mean shape and evolution are strongly affected by the interaction of the flow with the walls and the presence of recirculation zones in the combustion chamber (see Figure 1). Here, we propose a flow model which is based on experimental and numerical observations of the acoustically forced flow field. Then, we perform a qualitative comparison between the forced response of flame and heat release dynamics of our model and results obtained in previous studies. We then discuss our results and comment on how our low-order model could be improved in a future work. Once a satisfactory agreement with the realistic forced response is achieved, the flame-flow model can be coupled with a linear acoustic network as in [8], to obtain a flame-acoustic feedback loop and have a complete low-order thermoacoustic model able to predict frequencies and amplitudes of oscillations both in the frequency and time domain with a small computational cost.

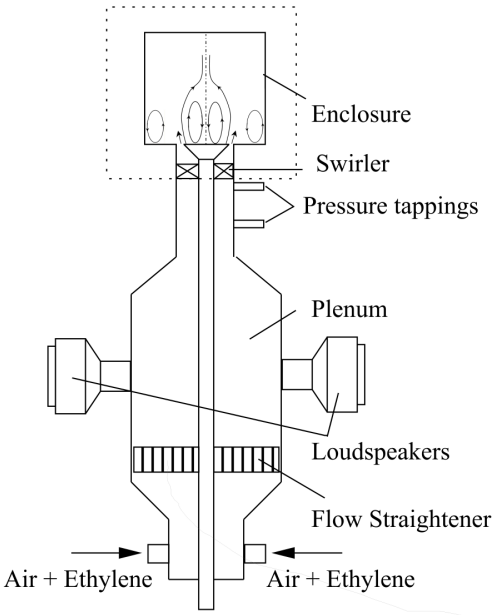

FIGURE 1: SCHEMATIC OF THE BLUFF-BODY COMBUSTOR RIG DEVELOPED BY [9]. AIR AND FUEL ARE PREMIXED FAR UPSTREAM OF THE DUMP PLANE. A SCHEMATIC OF THE FLOW FIELD IN THE COMBUSTION ZONE IS SHOWN.

MODELLING

In this section we describe in detail the low-order model and our assumptions. The main concept is to first obtain a mean flow representative of the geometry under consideration and freeze it, thus solving only for the linearized acoustic equations which induce fluctuations in the mean flow. As a consequence, the full Navier–Stokes equations need to be solved only once, for the mean flow, greatly reducing the computational cost needed. The geometry we consider is axisymmetric, and we will therefore use cylindrical polar coordinates.

Flow Field

We decompose the flow field $\boldsymbol{u}$ into a mean component $\overline{\boldsymbol{u}}$ and a fluctuation $\boldsymbol{u}'$. The latter is not necessarily small, as we will perform a nonlinear analysis. In the literature, most low-order analyses involving a kinematic description of the flame assume the mean flow to be uniform in the axial direction, and zero in the radial and azimuthal components. However, for the combustor we are modelling, we cannot make this assumption: the presence of a conical bluff-body just upstream the combustion

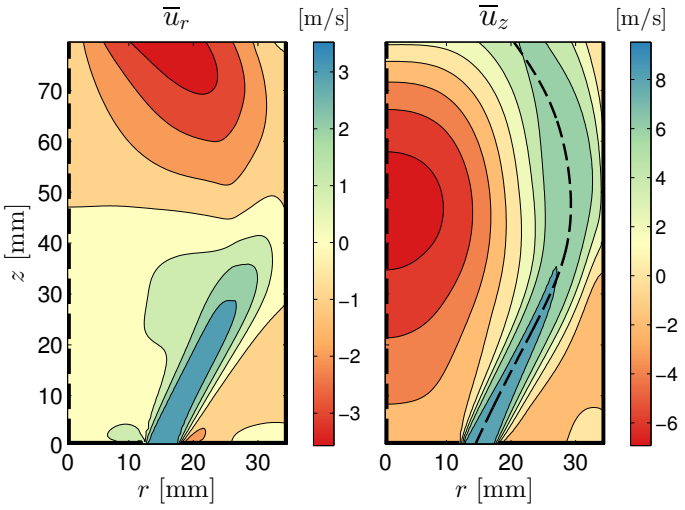

FIGURE 2: AVERAGED URANS FLOW FIELD COMPONENTS IN THE COMBUSTION ZONE. SOLID THICK LINES INDICATE WALLS. THE DASHED LINES INDICATE THE CENTERLINE (LEFT BOUNDARIES) AND THE STREAMLINE $r = \rho_s(z)$ THAT PASSES THROUGH THE SLOT MIDPOINT (ONLY IN THE RIGHT PANEL).

zone introduces a strong radial component of the flow at the inlet, creating a side recirculation zone at the dump plane. Also, the wake induced by the bluff body forms a large central recirculation zone. These recirculation zones guarantee the flame stabilization, as they promote flame anchoring at the dump plane, and also greatly affect the flame's shape and dynamics.

On account for this, we want to use a realistic mean flow, *i.e.*, a mean flow that accurately describes the location of the recirculation zones. This can be obtained solving the Reynolds-averaged Navier–Stokes (RANS) equations in the enclosed domain of Figure 1. The mean flow we use in the following analysis has been obtained by time-averaging unsteady RANS simulations performed by Armitage *et al.* and described in [11]. The radial ($\overline{u}_r$) and axial ($\overline{u}_z$) components of the averaged velocity field are shown in Figure 2, and the azimuthal component is zero, because we are considering a perfectly axisymmetric configuration.

On top of the mean flow, fluctuations develop when the system is acoustically forced by a loudspeaker, or when a thermoacoustic oscillation arises. Experimental cold flow smoke visualizations have shown that acoustic fluctuations cause the formation of a pair of counter rotating vortices in the inner and outer sides of the flame (one in each recirculation zone) [9]. The vortices are transported downstream with a characteristic velocity, the convection speed, causing flame wrinkling and consequent heat release fluctuations. The scenario is similar to the one observed for conical flames: in that case, oscillations are axisymmetric with respect to the centerline, and it has been shown that an axial developing travelling wave velocity model, with radial fluctuations computed by means of mass conservation, allows for a realistic description of the flame-flow coupling mechanism [1,2,3].

Mimicking this description, we want to generate a fluctuating flow field which is convected axially with a certain convection speed and generates vorticity in the inner and outer sides of the flame. For the axial component, we impose acoustic velocity fluctuations at the inlet, and we convect them downstream. For the convection, we use as a reference velocity the axial velocity of the streamline $r = \rho_s(z)$ that passes through the centre of the slot (see Figure 2). This assumes that axial fluctuations do not vary in the radial direction. Finally, we solve for mass conservation to obtain radial fluctuations. We want these oscillations to have opposite sign on the two sides of the flame, in order to emulate the formation of counter rotating vortices. This is achieved by imposing radial fluctuations to be zero along the streamline $r = \rho_s(z)$. Summarizing, we solve

$$\frac{\partial u'_z}{\partial t} + \overline{u}_z\left(\rho_s\left(z\right), z\right) \frac{1}{K} \frac{\partial u'_z}{\partial z} = 0, \qquad u'_z\left(z,t\right)|_{z=0} = u'_{ac}(t) \tag{1}$$

for the convection, and

$$\frac{1}{r}\frac{\partial\left(r u'_r\right)}{\partial r} + \frac{\partial u'_z}{\partial z} = 0, \qquad u'_r\left(r,z,t\right)|_{r=\rho_s(z)} = 0 \tag{2}$$

for mass conservation. The parameter K introduced in Eq. (1) is the ratio between the mean and convection speeds, which in general may not be equal to 1 [2, 13]. In the following, we fix $K = 1.5$; this particular choice for K is discussed in the *Convection Speed* section.

As we have assumed that axial fluctuations are not a function of the radial direction, Eq. (2) can be solved yielding an expression for radial fluctuations, which reads:

$$u'_r(r,z,t) = -\frac{1}{2}\frac{\partial u'_z}{\partial z} r \left(1 - \frac{\rho_s^2\left(z\right)}{r^2}\right). \tag{3}$$

Note that, with this model, radial fluctuations diverge when approaching the centerline $r = 0$. However, because we use a kinematic equation for the dynamics of the flame (see next section), we need to evaluate the velocity field only around the flame front, which is always distant from the centerline, and the use of Eq. (3) is justified.

Flame Model

We use the kinematic G-equation to describe the flame and heat release dynamics. We define a field G whose level set $G = 0$

identifies the flame surface, which separates reactants ($G<0$) from products ($G>0$). The flame front evolves according to the transport equation [14]:

$$\frac{\partial G}{\partial t}+\boldsymbol{u}\cdot\nabla G=s_L|\nabla G|. \tag{4}$$

Aside for its sign, the G-field away from the zero contour line has no physical meaning, and we define it as a signed distance function. We define the zero level set line implicitly, *i.e.*, as $G(r,z,t)=0$, without assuming that the flame is single-valued in one of the two coordinates as is done in [2,10]. This allows us to naturally describe topological changes in the solution, which occur when pocket of fuels detach from the flame's main body, and to be able to describe very wrinkled flame shapes, which in general cannot be found with an explicit treatment of the flame front. Topological changes and highly wrinkled structure are the main features of this flame, as can be observed in Figures 5 and 6, and need to be accounted for. In Eq. (4) $\boldsymbol{u}=\overline{\boldsymbol{u}}+\boldsymbol{u}'$ is the underlying flow field and s_L the flame speed. The flame speed is in general a function of the equivalence ratio, turbulence intensity, and local stretch effects. In this study, we consider fully premixed, laminar flames. The equivalence ratio ϕ is used to define the flame speed of the laminar flat flame sheet, which is given by the empirical relation:

$$s_L^0(\phi)=A\phi^B e^{-C(\phi-D)^2}. \tag{5}$$

The fuel we consider is an air-ethylene gaseous mixture, for which the coefficients in Eq. (5) are given by $A=1.32176$, $B=3.11023$, $C=1.72307$, $D=0.36196$ [11]. We consider a uniform equivalence ratio $\phi=0.65$, yielding $s_L^0=0.3$ m/s. Corrections to the unstretched flame speed are due to curvature effects, and are typically accounted for by [15]:

$$s_L=s_L^0(1-\mathscr{L}\kappa), \tag{6}$$

where $\mathscr{L}$ is the Markstein length and $\kappa=\nabla\cdot\hat{\boldsymbol{n}}=-\nabla\cdot\frac{\nabla G}{|\nabla G|}$ the flame curvature. We fix $\mathscr{L}=1.2\cdot10^{-3}$ m; this value is consistent with the Markstein numbers which have been used in similar studies on the conical flame modelled with the G-equation [7,8]. However, Eq. (6) is a linear correction to the flame speed with respect to the local curvature. Looking at the flame shapes that were observed experimentally and numerically, we expect to find very wrinkled flame structures and the formation of pinch-offs. When a pinch-off forms, the flame becomes cuspy and the local curvature can be very high: higher-order stretch corrections are needed. Other studies [16,17] have addressed the question of developing nonlinear models for the influence of highly stretched

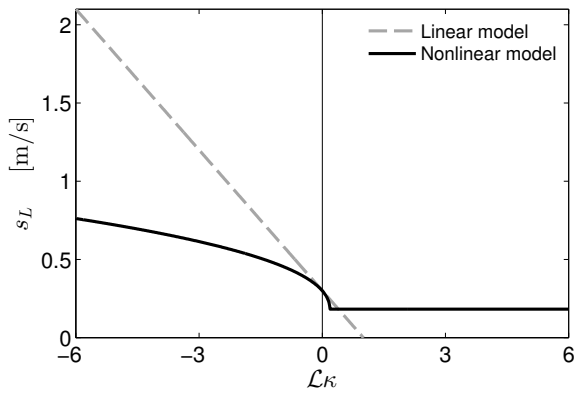

FIGURE 3: NONLINEAR MODEL ADOPTED FOR THE FLAME SPEED CURVATURE DEPENDENCE FOR $s_L^0=0.3$. HIGH-ORDER TERMS DECREASE THE CURVATURE'S INFLUENCE ON THE FLAME SPEED.

flame sheets on the flame speed. We shall adopt one of the nonlinear models they have proposed, which reads:

$$s_L(\kappa):\begin{cases}\left(\frac{s_L}{s_L^0}\right)^2\log\frac{s_L}{s_L^0}=-\mathscr{L}\kappa & \kappa\le\frac{1}{2\mathscr{L}e}\\ s_L=s_L^0e^{-\frac{1}{2}} & \kappa>\frac{1}{2\mathscr{L}e}\end{cases}, \tag{7}$$

and is plotted in Figure 3. In Eq. 7 the flame speed s_L is defined implicitly as a function of the curvature κ.

Expanding Eq. (7) around $s_L=s_L^0$ (*i.e.*, small curvature) yields:

$$\kappa(s_L)\approx-\frac{1}{\mathscr{L}}\left[\kappa|_{s_L=s_L^0}+\left.\frac{d\kappa}{ds_L}\right|_{s_L=s_L^0}\left(s_L-s_L^0\right)\right]=$$
$$=-\frac{1}{\mathscr{L}}\frac{s_L-s_L^0}{s_L^0}, \tag{8}$$

showing that in this limit we recover the linear model (6). The saturation in Eq. (7) for $\kappa>1/(2\mathscr{L}e)$ is necessary to keep the flame speed single-valued with respect to the curvature. Nevertheless, it is unlikely that curvature values will lie within this range because premixed flames propagate normal to themselves and cusps form pointing towards the products [18]. Large positive curvature values would indicate that a cusp has formed pointing towards the reactants, which is unlikely to arise and can be checked afterwards. Adopting the nonlinear model (7), the influence that the curvature has on the flame speed is reduced for very wrinkled flame sheets.

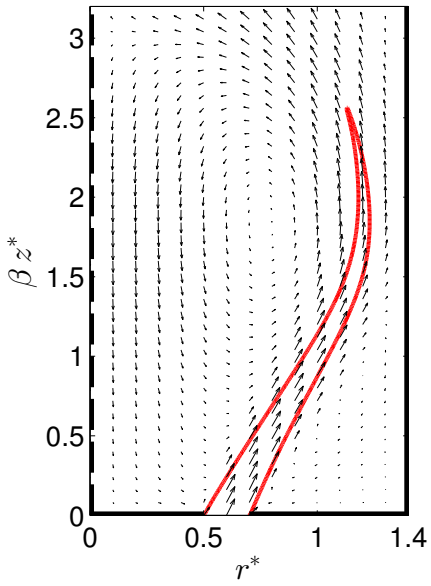

FIGURE 4: MEAN FLAME SHAPE CONTOUR $G = 0$ (RED LINE) AND MEAN FLOW VECTOR PLOT FOR $\phi = 0.65$, $\mathscr{M} = 0.015$.

Numerical Implementation and Mean Flame Shape

To numerically integrate Eq. (4) we define the following set of non-dimensional variables:

$$t^* = t\frac{u_{ref}}{H} \qquad \boldsymbol{u}^* = \frac{\boldsymbol{u}}{u_{ref}} \qquad s_L^* = \frac{s_L}{u_{ref}}$$
$$z^* = \frac{z}{H} \qquad r^* = \beta\frac{r}{H} \qquad \mathscr{M} = \frac{\mathscr{L}}{H} \tag{9}$$

where $\beta = H/D$, H and D are the enclosure height and the diameter of the bluff body respectively (see Figure 1), and u_{ref} is a reference speed chosen to be the one at the slot midpoint. In contrast to the G-equation notation widespread in the literature, in which the stretch parameter β represents the flame's aspect ratio [2, 6], here β does not have a particular physical meaning and is just a geometrical parameter. This is because the mean flow is non-uniform and therefore we cannot derive an analytical expression that relates the flame's aspect ratio to the flame speed.

Setting $H = 80$ mm, $D = 25$ mm, and $u_{ref} = 10$ m/s, we fully determine the non-dimensional variables in (9). The numerical method we use to integrate Eq. (4) is a well-established technique for the integration of level sets, the Narrow Band Level Set Method, described by [19]. Details on our numerical implementation can be found in [20, 6, 7, 8].

Figure 4 shows the G-field zero level set obtained by setting the acoustic fluctuations $u'_{ac} = 0$ in Eq. (1), thus solving the stationary problem:

$$\beta\overline{u}_r{}^*\frac{\partial G}{\partial r^*} + \overline{u}_z{}^*\frac{\partial G}{\partial z^*} = s_L^*(\kappa)\sqrt{\left(\beta\frac{\partial G}{\partial r^*}\right)^2 + \left(\frac{\partial G}{\partial z^*}\right)^2}. \tag{10}$$

The steady flame shape compares favourably with the shapes that have been computed numerically by RANS simulations [11, 12]. This steady solution is used as an initial condition in the following analysis.

FORCED ACOUSTIC RESPONSE

For the enclosure length we have considered ($H = 80$ mm), the system is thermoacoustically stable. Consequently we investigate the forced (rather than self-excited) response of the system to axial flow oscillations. This will allow us to compare the unsteady flame structures and heat release response predicted by the low-order model with the ones observed experiments and URANS simulations.

We force the system by imposing velocity fluctuations of amplitude $A = [0.1\,,\,3.0]$ m/s and frequency $f = [40\,,\,500]$ Hz at the inlet of the domain, *i.e.*, by setting the boundary condition of Eq. (1) to

$$u'_{ac}{}^*(t^*) = \varepsilon\sin(2\pi St\,t^*)\,, \tag{11}$$

where we have defined the non-dimensional amplitude of forcing $\varepsilon = A/u_{ref}$, and the Strouhal number $St = fH/u_{ref}$.

We numerically integrate the system forward in time for a time sufficient to reach the steady-state response and compute a few limit cycles on it.

Qualitative Comparison

As our model is low-order, we do not expect a quantitative agreement with the experimental results. We are nevertheless interested in a qualitative comparison, in order to understand whether the model is capturing the main physical features of the system.

We focus the discussion on the two cases forced at a frequency $St = 1.28$ ($f = 160$ Hz) and amplitudes $\varepsilon = 0.1, 0.25$. In Figures 5 and 6, we compare our instantaneous flame fronts and velocity vector fields with those of Armitage *et al.*'s URANS simulations[1] [11] at three phase angles over a forced cycle. A comparison with the simulations is easier, because we can compare the flame front G=0 from our simulations with the contour lines of URANS snapshots corresponding to the $c = 0.5$ isocontour of the progress variable, which is a good indicator of the flame front position. Experimental results only provide OH chemiluminescence fields, which are difficult to compare with

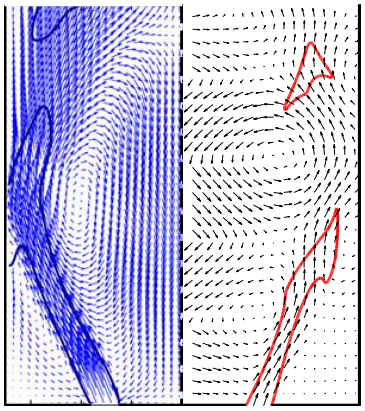

(a) $\varphi_{\text{cycle}} = \pi/6$

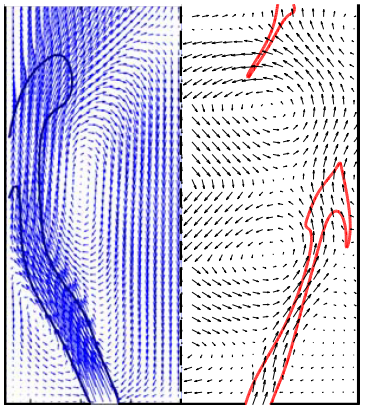

(b) $\varphi_{\text{cycle}} = 3\pi/6$

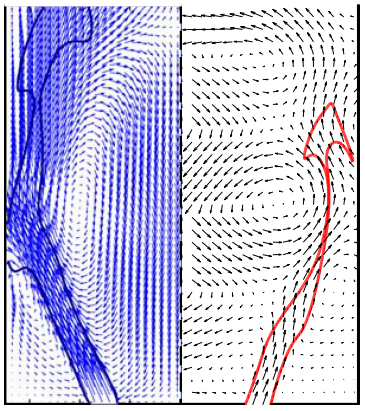

(c) $\varphi_{\text{cycle}} = 5\pi/6$

FIGURE 5: COMPARISON BETWEEN (LEFT) URANS AND (RIGHT) LOW-ORDER MODEL FLAME SHAPES AND FLOW FIELDS OVER A FORCING CYCLE WITH $St = 1.28$, $\varepsilon = 0.1$.

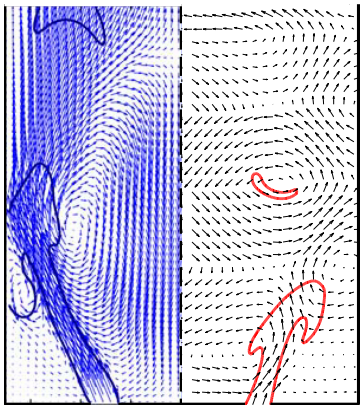

(a) $\varphi_{\text{cycle}} = \pi/6$

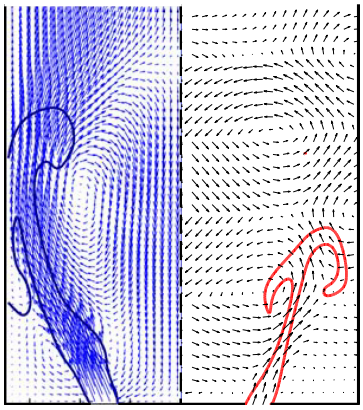

(b) $\varphi_{\text{cycle}} = 3\pi/6$

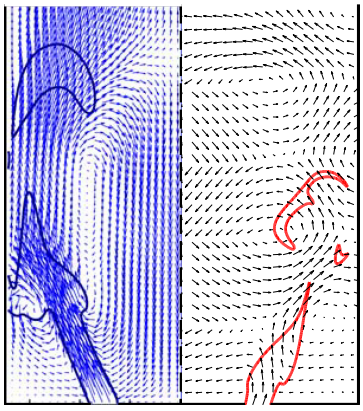

(c) $\varphi_{\text{cycle}} = 5\pi/6$

FIGURE 6: COMPARISON BETWEEN (LEFT) URANS AND (RIGHT) LOW-ORDER MODEL FLAME SHAPES AND FLOW FIELDS OVER A FORCING CYCLE WITH $St = 1.28$, $\varepsilon = 0.25$.

the G-field, because the latter has no physical meaning away from the flame surface. An indirect comparison with the experiments can be found in [11].

At small forcing amplitudes (Figure 5), the intensity of the vortices is fairly small, and the flame tends to be long, undergoing a severe stretching. This eventually creates a large pinch-off which detaches from the flame far downstream and is then advected while burning; this large pocket of reactants does not burn completely before exiting the computational domain, meaning that part of the heat release is not accounted for. However, the latter problem is found also in DNS simulations and in the experiments, where the domain of computation of heat release is limited by the camera window for the OH chemiluminescence measurements.

At higher amplitudes (Figure 6), the flame structure over a cycle is very different. As the strength of the vortices is higher, the flame pinches off at a shorter axial distance, and as a consequence the flame is smaller on average. Also, the roll up of the vortices causes the formation of a characteristic mushroom-shape at the top of the flame, which we capture well. On the other hand, there are a few features that we cannot describe, such as the flame's impingement at the wall, which is responsible for some differences in the flame front shapes. Also, we note that the flames evaluated with the low-order model tend to be shorter than URANS flames. This is a common feature of all our simulations, and is probably due to the fact that we are not modelling gas expansion across the flame. The flame average length could be adjusted by varying the unstretched flame speed s_L^0 or the equivalence ratio as in Eq. (5). Also, we recall that the flow field model has to be valid only close to the flame surface, and no comparison should be sought far away from the $G=0$ lines.

Although improvements are possible, we find that the low-order flame-flow interaction model gives a reasonable description of the main kinematic features of the flame front, and it represents a significant improvement in the description of this type of flames respect to previous models involving the G-equations, such as the one presented in [10].

Heat Release Response

The heat release response is computed by calculating the amount of fuel burned at every instant in the domain, by

$$Q = 2\pi\rho h_r \int_0^R \int_0^H s_L(\kappa)\sqrt{\left(\frac{\partial G}{\partial r}\right)^2 + \left(\frac{\partial G}{\partial z}\right)^2}\,\delta(G)\,r\,dr\,dz, \quad (12)$$

where δ is the Dirac delta function. The non-dimensional heat release fluctuations are defined by $q' = (Q-\overline{Q})/\overline{Q}$, where $\overline{Q}$ is the heat release averaged over a forcing cycle.

The integrated heat release over a forced cycle with $St = 1.28$ and $\varepsilon = 0.1$ is shown in Figure 7. The heat release

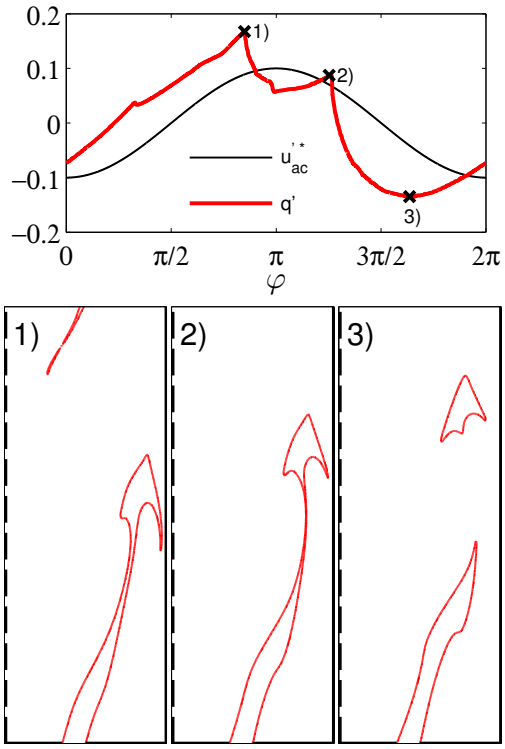

FIGURE 7: HEAT RELEASE RESPONSE OVER A FORCED CYCLE WITH $St = 1.28$ AND $\varepsilon = 0.1$. FLAME FRONT SNAPSHOTS CORRESPONDING TO KEY MOMENTS IN THE HEAT RELEASE RESPONSE.

signal is strongly non-harmonic, showing that that heat release is a strongly nonlinear function of the imposed velocity. The amplitude of heat release oscillations is greater than the amplitude of the forcing, meaning that the gain of the system exceeds 1, and the two oscillations are about $\pi/2$ out of phase.

A few key points of the heat release response have been highlighted in Figure 7. Point 1) corresponds to the absolute maximum of the heat release response, and is one of the cusps in the signal. To gain insight into the physical causes of the appearance of sharp peaks, we have plotted in the corresponding bottom panel of Figure 7 the flame front at the same instant. The main body of the flame is quite stretched, and there is a pocket of fuel, which had been released during the previous cycle, that is exiting the domain. On closer inspection, one can see that, at the instant under consideration, this pocket of fuel is breaking into two parts, which means that the flame has just pinched off. A pinch-off creates a discontinuity in the flame shape, and the local flame curvature close to the pinch-off location suddenly becomes highly negative. Thus, according to Eq. (7), the local flame speed becomes higher. This has two effects:

a. from Eq. (12) we see that the flame speed directly enters

[1]Reprinted from [11], with permission from Elsevier.

into the evaluation of heat release fluctuations. Therefore, it is expected that the moment at which the flame pinches off corresponds to an instantaneously high heat release response;

b. at the same time, a higher flame speed increases the rate of kinematic restoration (kinematic restoration is the process that smooths out the flame's wrinkles, and it is due to the fact that the flame propagates normal to itself [18]). As a consequence, the cusps formed on the flame front are smoothed out quickly, decreasing the magnitude of curvature corrections and destroying flame surface area. Because both these effects have a negative impact on the total heat released by the flame, a rapid decrease of q' is expected after a pinch-off.

This is consistent with our observations. The same features just discussed are observed also in the second peak of the heat release time series, at point 2), where the main body of the flame undergoes a pinch-off. Finally, point 3) is the absolute minimum of q', as it corresponds to a moment in which the flame is short, and cusps on the flame surface have been smoothed out by kinematic restoration. From this instant on, the flame will elongate, increasing flame surface and thus heat release, until point 1) is reached again and the cycle restarts.

These arguments suggest that, for this particular flame's structure, the formation of pinch-offs has an important role in the heat release response, because it induces high amplitude fluctuations and the formation of cusps in the time-signal, which enhance nonlinear effects. Note that this effect cannot be observed in the simpler configuration of a conical flame [7, 8]. For conical flames, pinch-offs occur at the centerline $r = 0$: because the flame is axisymmetric, the contribution of a flame element to the heat release is proportional to the radial distance (see Eq. (12)), and even if the local flame structure is highly wrinkled, its weight on the evaluation of the heat release is negligible. On the other hand, for the flame under consideration in this study, pinch-offs occur at a large radial distances, and provide large contributions to the integration of total heat release.

Flame Describing Function Having integrated the forced response of heat release to velocity fluctuations, we can evaluate the Flame Describing Function (FDF) for this flame-flow configuration. The FDF is evaluated by extracting the heat released at the forcing frequency q_1, neglecting higher harmonics, and is calculated by:

$$\mathscr{F}(St,\varepsilon) = G_1(St,\varepsilon)\, e^{\mathrm{i}\phi_1(St,\varepsilon)}, \tag{13}$$

where i is the imaginary unit, $G_1(St,\varepsilon) = \left|\frac{\hat{q}_1(St,\varepsilon)}{\varepsilon}\right|$ and $\phi_1(St,\varepsilon)$ are respectively the gain and phase of the heat release first harmonic component to inlet velocity fluctuations.

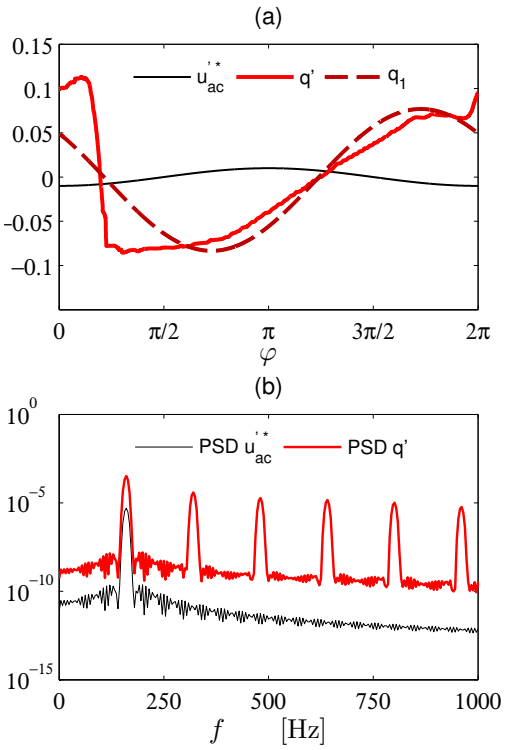

FIGURE 8: (a): HEAT RELEASE RESPONSE OVER A FORCED CYCLE WITH $St = 1.28$ AND $\varepsilon = 0.01$. THE CONTRIBUTION OF THE FIRST HARMONIC IS HIGHLIGHTED. (b): PSD OF VELOCITY AND HEAT RELEASE FLUCTUATIONS.

Figure 8 (a) shows the heat release signal (and its first harmonic component) when the system is forced at 160 Hz with the smallest amplitude we have considered, $\varepsilon = 0.01$: although the forcing amplitude is small, it is sufficient to induce the formation of pinch-offs, which is a nonlinear effect. This causes heat release fluctuations to have a very large amplitude, and the system's gain exceeds 1 by a large amount. Note that in experiments and URANS simulations the system response is linear for this forcing amplitude; this suggests the the low-order model is too nonlinear, and corrections should be done to prevent the formation of pinch-offs at small forcing amplitudes. The presence of cusps in the heat release signals causes higher harmonics to have large contributions. The PSD plot of heat release fluctuations in Figure 8 (b) shows how strong the contribution of higher harmonics is even at this small forcing amplitude. Thus, if we want to use this FDF in a thermoacoustic feedback loop, we must assume that higher harmonics in the heat release are filtered out by the acoustic transfer function, which has to act as a strong low-pass for the feedback loop analysis to work (this assumption is not required if one uses time-domain techniques such as continuation

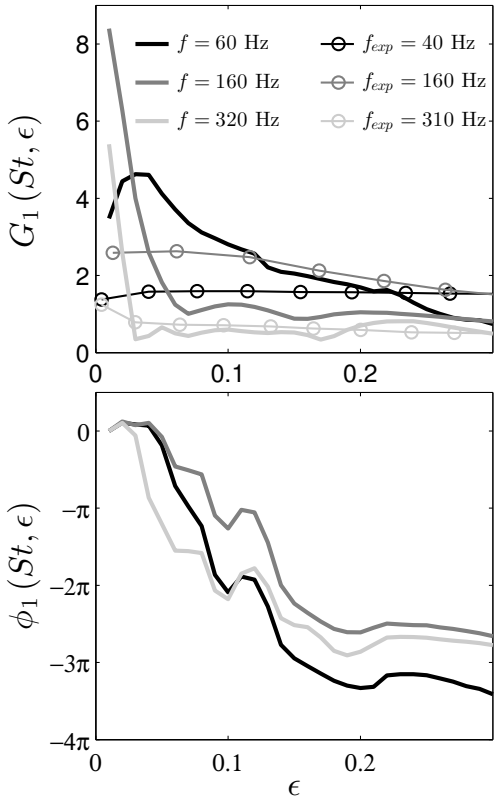

FIGURE 9: FDF GAIN AND PHASE AS A FUNCTION OF THE FORCING AMPLITUDE AT THE FREQUENCIES $St = 0.48, 1.28, 2.56$. THICK LINES CORRESPOND TO THE LOW-ORDER MODEL RESULTS, CIRCLES TO EXPERIMENTAL MEASUREMENTS.

analysis [7, 8]).

Figure 9 shows the FDF amplitude dependence for three forcing frequencies. As discussed earlier, the phase is affected by the convection speed value we have chosen, and will not be further discussed.

For all the frequencies we have considered, the gain shows an overall monotonical behaviour with the amplitude, which is in agreement with experimental measurements. At small amplitudes the gain exceeds the unitary value for all the frequencies shown. This is expected (to some extent) because of the similarity between this flame shape and V shaped flames [1, 3]. In the linear limit, we find that the gain increases with the forcing frequency, reaches a maximum value at a forcing of 160 Hz, and then decreases for higher frequencies; the same feature was observed in experimental and URANS investigations [9, 11, 12]. By the linear limit we mean the smallest forcing amplitude we have considered, $\varepsilon = 0.01$. Nevertheless, as we have shown that pinch-offs can form at this amplitude, inducing nonlinear effects, the behaviour of the system in the linear limit is not properly characterised, and simulations with even smaller forcing amplitudes need to be performed, or the contribution of pinch-offs on the heat release has to be reduced.

We note that the gain values we find are much higher than those of the real system, especially in the low amplitude limit. The gain reaches a maximum value of about 8, against the maximum value of 3 found in experiments at the same frequency. Excluding the influence of pinch-offs on the heat release that we have already discussed, a second possible explanation for such a strong overestimation of the gain can be found in the lack of a turbulence model in the underlying flow field in our equations. Indeed, in [21, 22] it has been shown that, because of nonlinearities in the governing equations, turbulent fluctuations modelled as stochastic fluctuations couple with the forced oscillations and flame dynamics, affecting the kinematic restoration process, hence the formation of cusps, the rate at which flames wrinkles are smoothed out, and the evolution of the heat release.

CONVECTION SPEED

In order to have a qualitatively reasonable comparison between URANS and low-order simulations in Figures 5 and 6, we have only looked at the flame's structures. As it turns out, this results in a disagreement between the velocity phases of the images we have compared. For the URANS simulations, the starting point of the limit cycle corresponds to a minimum in the velocity fluctuations at the slot; we denote this condition as φ^0_{min}. For the low-order simulations, we find that the phase that allows for a good comparison of flame fronts does not correspond to φ^0_{min}, but it has a shift $\Delta\varphi \approx \pi/4$ rad.

This shift is likely to be caused by our choice for the convection speed of velocity fluctuations. Indeed, several studies have shown that this parameter plays a key role in the correct description of the dynamics [2, 13]. In the advection Equation (1) we have chosen the ratio between the mean and convection velocities to be $K = 1.5$. This was based on DNS simulations performed by [13], which predicted a value of K in the range $[1.1\,, 2.0]$; values in this range have already been used in other studies [7, 6, 8]. However, the latter results were obtained for a laminar, conical flame configuration, and it is not surprising that the value of the convection speed may significantly vary for a bluff-body stabilized, turbulent flame. We nevertheless used laminar flame results because of the lack of information on the convection speed for the dump combustor under investigation when we started this study. More recently, new experiments have been performed on the same combustor by [23]. Applying Proper Orthogonal Decomposition (POD) analysis on phase-averaged OH^* chemiluminescence images and computing the Power Spectral Density (PSD) of the POD time coefficients on self-excited thermoacoustic cycles, they have estimated the ratio between the mean flow and the convection speeds to be in the range $K = [0.59\,, 0.72]$. Unfortunately this information was not available to us when we

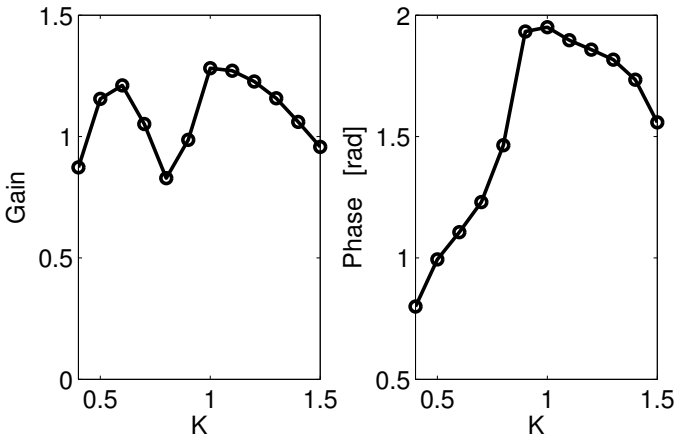

FIGURE 10: EFFECT OF THE CONVECTION SPEED ON THE HEAT RELEASE GAIN AND PHASE RESPONSE. FORCING AMPLITUDE AND FREQUENCY HAVE BEEN FIXED TO $\varepsilon = 0.25$ AND $St = 1.28$ RESPECTIVELY.

performed the numerical simulations for the calculation of the FDF. A lower value of K means that fluctuations are advected downstream with a velocity that on average is higher than that of the mean flow, whereas in our calculations we have assumed them to move more slowly. A smaller convection speed corresponds to a larger wavelength between two vortices on the same side of the flame. This has a direct impact on the phase between the shedding of the vortices and the flame structure over time, and thus on the formation of pinch-offs and the heat release phase with respect to velocity fluctuations. It is worth mentioning that the convection speed is in general a function of the frequency (as found by [13]), and the analysis performed by [23] is not exhaustive, as it is performed on self-excited oscillations, which tend to have a frequency of about 350 Hz, close to the first resonant frequency of the burner.

Having gained knowledge of experimentally determined values for the convection speed, we have performed some numerical simulations fixing the amplitude and frequency of inlet oscillations, and varying the parameter K in the range $[0.4, 1.5]$ in steps of $\Delta K = 0.1$. To quantify the impact of K on the dynamics of the flame, we show in Figure 10 the gain and phase dependence on K of the FDF (defined as in Eq. (13)) evaluated at $\varepsilon = 0.25$ and $f = 160$ Hz. The phase follows a clear path: it reaches a maximum when the convection speed is $K = 1$ and monotonically decreases for other values of K. Looking at the phase values for $K = 1.5$ (our simulations), and $K = 0.6$ (experimentally determined), we observe that we can correct the phase of heat release fluctuations of about $\pi/6$ rad. On the other hand, the gain has an oscillatory dependence with respect to the convection speed, and the system's amplitude response is very sensitive to variations in K. Nevertheless, these variations are not enough to explain the strong gain overestimation we have observed in Figure 9.

1 Conclusions

In this study we have developed a low-order model to investigate the forced response of a bluff-body stabilized dump combustor, with a view to perform low-order analysis on self-excited oscillations in this combustor in the future. The flame front has been described by the kinematic G-equation evolving in a non-uniform flow field, which has been computed with URANS simulations. We have attempted to extend the classical travelling wave model that describes the interaction between conical flames and flows to this configuration. The model has been developed by analyzing experimentally determined cold flow smoke visualizations of the forced system.

The resulting forced dynamics has been investigated by examining the system's response over a cycle: although a quantitative comparison cannot be performed because of fundamental differences between the systems, an acceptable qualitative agreement between URANS and low-order flame shapes is found, meaning that our model captures the main kinematic features of the flame surface dynamics, such as the formation of distorted mushroom-shaped fronts and pinch-offs. We have evaluated the Flame Describing Function (FDF) to inlet velocity fluctuations, and shown its amplitude dependence for three forcing frequencies. The dependence of the gain on the amplitude and frequency qualitatively compares favorably with experimental results, but we overestimate by a large amount the system's gain. This can have two causes. First, we find that pinch-offs form even at fairly small forcing amplitudes for this flame's structure, and they have a major role in the description of the flame and heat release dynamics. In particular, because they create cuspy flame fronts, they lead to large maximum values in the heat release, followed by a rapid destruction of flame surface. This occurs even if we have adopted a nonlinear model for the flame speed dependence on the curvature, which reduces the importance of very wrinkled flame fronts on the flame dynamics and heat release evaluation. As a consequence, the amplitude of heat release fluctuations is enhanced, and peaks in its signal are created, which in turn augments the heat release nonlinear response. This is a characteristic of this flame shape, and cannot be observed on conical flames, where pinch-offs occur at the centerline and have a very small influence on the heat release evaluation. The second cause of the gain overestimate is probably due to the lack of a turbulent model for the flow field, which has a non-negligible impact on the flame and heat release dynamics.

The level of reliability of the low-order model can be improved. The convection speed of velocity perturbations can be varied according to the latest experimental results on the experimental apparatus. Preliminary results show that adjusting the convection speed to experimentally determined values has a strong effect on the system gain and phase response. In particu-

lar, it improves the agreement between the phases of heat release and velocity fluctuations, but cannot address the overestimation of the gain. The impact of pinch-offs on the heat release response can be reduced by varying the value of the Markstein length. Finally, a stochastic component can be added to the flow field to emulate turbulence effects. The latter two changes should reduce the heat release gain response to velocity fluctuations. The qualitative agreement obtained so far is encouraging for further research on this model. If the further modifications proposed in this paper prove satisfactory, the flame-flow model could then be used as a reliable, low-cost tool that can be coupled with an acoustic solver in order to obtain a complete low-order thermoacoustic network.

ACKNOWLEDGMENT

The authors thank Dr C. Armitage for having shared results of URANS simulations. This project was founded by the European Research Council through Project ALORS 2590620.

REFERENCES

[1] Schuller, T., Durox, D., and Candel, S., 2003. "A unified model for the prediction of laminar flame transfer functions: comparisons between conical and V-flames dynamics". *Combustion and Flame,* ***134***(1-2), July, pp. 21–34.

[2] Preetham, Hemchandra, S., and Lieuwen, T., 2008. "Dynamics of laminar premixed flames forced by harmonic velocity disturbances". *Journal of Propulsion and Power,* ***24***(6), Nov.-Dec., pp. 1390–1402.

[3] Durox, D., Schuller, T., Noiray, N., and Candel, S., 2009. "Experimental analysis of nonlinear flame transfer functions for different flame geometries". *Proceedings of the Combustion Institute,* ***32***(1), Jan., pp. 1391–1398.

[4] Dowling, A., 1999. "A kinematic model of a ducted flame". *Journal of Fluid Mechanics,* ***394***, Sept., pp. 51–72.

[5] Noiray, N., Durox, D., Schuller, T., and Candel, S., 2008. "A unified framework for nonlinear combustion instability analysis based on the flame describing function". *Journal of Fluid Mechanics,* ***615***, Nov., pp. 139–167.

[6] Kashinath, K., Waugh, I., and Juniper, M., 2014. "Nonlinear self-excited thermoacoustic oscillations of a ducted premixed flame: bifurcations and routes to chaos". *Journal of Fluid Mechanics*. accepted.

[7] Waugh, I., Kashinath, K., and Juniper, M., 2014. "Matrix-free continuation of limit cycles and their bifurcations for a ducted premixed flame". *Journal of Fluid Mechanics,* ***759***, pp. 1–27.

[8] Orchini, A., Illingworth, S., and Juniper, M., 2014. "Frequency domain and time domain analysis of thermoacoustic oscillations with wave-based acoustics". *Journal of Fluid Mechanics*. submitted.

[9] Balachandran, R., 2005. "Experimental investigation of the response of turbulent premixed flames to acoustic oscillations". PhD thesis, University of Cambridge.

[10] Graham, O., 2012. "Modelling the thermoacoustic response of premixed flames". PhD thesis, University of Cambridge.

[11] Armitage, C., Balachandran, R., Mastorakos, E., and Cant, R., 2006. "Investigation of the nonlinear response of turbulent premixed flames to imposed inlet velocity oscillations". *Combustion and Flame,* ***146***(3), Aug., pp. 419–436.

[12] Ruan, S., Dunstan, T., Swaminathan, N., and Balachandran, R., 2013. "Computation of turbulent premixed flames response to inlet velocity oscillation". In 24th International Colloquium on the Dynamics of Explosions and Reactive Systems.

[13] Kashinath, K., Hemchandra, S., and Juniper, M., 2013. "Nonlinear thermoacoustics of ducted premixed flames: the influence of perturbation convection speed". *Combustion and Flame,* ***160***, Dec., pp. 2856–2865.

[14] Markstein, G. H., 1964. *Non-steady flame propagation*. Pergamon.

[15] Tien, J., and Matalon, M., 1991. "On the burning velocity of stretched flames". *Combustion and Flame,* ***8***, pp. 238–248.

[16] Ronney, P., and Sivashinsky, G., 1989. "A theoretical study of propagation and extinction of nonsteady spherical flame fronts". *SIAM J. Appl. Math.,* ***49***(4), pp. 1029–1046.

[17] Kelley, A. P., and Law, C., 2009. "Nonlinear effects in the extraction of laminar flame speeds from expanding spherical flames". *Combustion and Flame,* ***156***, Sept., pp. 1844–1851.

[18] Lieuwen, T., 2012. *Unsteady combustor physics*. Cambridge University Press.

[19] Sethian, J., 1999. *Level Set methods and Fast Marching methods*, 2nd ed. Cambridge University Press.

[20] Hemchandra, S., 2009. "Dynamics of turbulent premixed flames in acoustic fields". PhD thesis, Georgia Institute Technology.

[21] Hemchandra, S., Peters, N., and Lieuwen, T., 2011. "Heat release response of acoustically forced turbulent premixed flamesrole of kinematic restoration". *Proceedings of the Combustion Institute,* ***33***(1), pp. 1609–1617.

[22] Shin, D., and Lieuwen, T., 2013. "Flame wrinkle destruction processes in harmonically forced, turbulent premixed flames". *Journal of Fluid Mechanics,* ***721***, Mar., pp. 484–513.

[23] Kypraiou, A., Dowling, A., Mastorakos, E., and Karimi, N., 2014. "Proper Orthogonal Decomposition analysis of a turbulent swirling self-excited premixed flame". *American Institute of Aeronautics and Astronautics*. submitted.